Magnetic Properties and Crystal Structures of 1,5-Diphenylverdazyls with Electron Acceptor Groups in the 3-Position

Masaki Mito and Kazuyoshi Takeda

Department of Applied Science, Faculty of Engineering, Kyushu University, Fukuoka 812, Japan

Kazuo Mukai and Nagao Azuma

Department of Chemistry, Faculty of Science, Ehime University, Matsuyama 790-77, Japan

Marco R. Gleiter, Claus Krieger, and Franz A. Neugebauer*

Arbeitsgruppe Organische Chemie, Max-Planck-Institut für medizinische Forschung, Jahnstr. 29, D-69120 Heidelberg, Germany

Received: July 7, 1997; In Final Form: August 27, 1997[⊗]

The magnetic properties of four diphenylverdazyls (**2**−**5**) with electron acceptor groups in the 3-position were studied by measuring the magnetic susceptibility and heat capacity. The crystal structures of **3** and **4** were determined, and for **2** the crystal structure analysis led to an improved refinement. Verdazyl **2** was found to be an antiferromagnet with a Neel temperature of $T_N = 1.16 \pm 0.04$ K. Above the transition temperature T_N, **2** behaves as a quasi-one-dimensional Heisenberg ferromagnet with the intrachain exchange interaction of $2J/k_B = +7.0 \pm 1.0$ K. The interchain exchange interaction zJ'/k_B was estimated to be -1.5 ± 0.2 K, where z is the number of interchain bonds per spin. On the other hand, **3** and **5** behave as 1D nonalternating and alternating Heisenberg antiferromagnets with an exchange interaction of $2J/k_B = -11.6$ K and $2J_1/k_B = -113$ K (alternation parameter $\alpha = J_2/J_1 = 0.4$), respectively. The susceptibility of **4** follows the Curie−Weiss law with a negative Weiss constant of −18 K above 100 K. Below 100 K, **4** showed anomalous magnetic behavior that cannot be explained by a simple model. The magnetic properties of **2**−**4** are discussed based on the results obtained by crystal structure analyses.

1. Introduction

In recent years, the quest for nonpolymeric ferromagnets has initiated extensive investigations of organic radicals in the solid state with regard to their magnetic ordering. However, ferromagnetic interactions have rarely been detected. Only very few compounds show a transition to a true ferromagnetic state, and furthermore, their Curie (transition) temperatures (T_c) are very low, $T_c < 2$ K. Representative examples are 4-[(1,1′-biphenyl-4-ylmethylene)amino]-2,2,6,6-tetramethyl-1-piperidinyloxy nitroxide ($T_c = 0.4$ K),[1] 1,3,5,7-tetramethyl-2,6-diazaadamantane-2,6-bis(yloxy) bisnitroxide ($T_c = 1.48$ K),[2] the β-phase of 4,5-dihydro-4,4,5,5-tetramethyl-2-(4-nitrophenyl)-1*H*-imidazol-1-yloxy 3-oxide (**1**) ($T_c = 0.60$ K),[3] and 3-(4-chlorophenyl)-1,5-dimethyl-6-thioxoverdazyl ($T_c = 0.68$ K).[4] Recently, an extensive study of a large range of TEMPO type nitroxides revealed that intermolecular ferromagnetic interactions are frequent in this radical group.[5] The ferromagnetic interactions in these nitroxides seem to be related to a characteristic molecular arrangement in the crystal, namely, to close contacts between the oxygen of an NO site and methyl and/or methylene hydrogens at the β-positions of adjacent NO moieties.[6] In this arrangement, the spin-alternation mechanism probably gives rise to the intermolecular ferromagnetic coupling.

Also, a range of 1,5-diaryl-substituted verdazyls has been searched for intermolecular ferromagnetic interactions.[7] The obtained results are rather poor. There is, however, one exception. Induced by the structural features of the nitronyl nitroxide β-**1**, F. Wudl et al.[8] synthesized 3-(4-nitrophenyl)-substituted verdazyls and discovered that 3-(4-nitrophenyl)-1,5,6-triphenylverdazyl (**2**) exhibits evidence of short-range ferromagnetic interactions. In the temperature region from 100 to 30 K the static magnetic susceptibility χ_M emu/mol follows the Curie−Weiss Law ($C = 0.382$ emu K/mol) with a positive Weiss temperature of +1.6 K. Below 30 K, χ_M deviates strongly from the Curie−Weiss law and shows a maximum ($\chi_M = 0.241$ emu/mol) at 2.15 K. The product $\chi_M T$ increases below 100 K and reaches a maximum (0.529 emu K/mol) at 3.9 K. These unusual magnetic properties were related to the results of a rough crystal structure determination ($R = 0.15$) of **2**.[8] Probably caused by the steric requirements of the 6-phenyl substituent being almost perpendicularly arranged with respect to the verdazyl nitrogen plane, the stacked molecules are mutually shifted along the C3···C6 axis and build up a stair pattern. In this structure the verdazyl ring with large positive spin populations at the nitrogens is in contact with the adjacent coplanar 4-nitrophenyl segment bearing very small positive and negative spin populations. An optimal arrangement of this kind shows the crystal structure of 1,3,5-triphenyl-6-oxoverdazyl in which the verdazyl ring and the 3-phenyl ring of adjacent molecules are lying alternately on top of each other.[9] For this compound, on the other hand, only weak ferromagnetism was detected below 4.9 K, which is attributed to a canting of the antiferromagnetic sublattices.[7f,g] In addition, the 1,3,5-triphenyl-6-oxoverdazyl shows nonresonant microwave absorption (MMMA).[7f] Encouraged by this observation, we checked a set of verdazyls available in our laboratory including **2**. The verdazyl **2**, however, gave no indication of MMMA down to 1.8 K. This point directed our interest to compound **2** and prompted us to improve its crystal structure determination and to characterize the low-temperature magnetic properties in more

[⊗] Abstract published in *Advance ACS Abstracts,* October 15, 1997.

S1089-5647(97)02195-0 CCC: $14.00

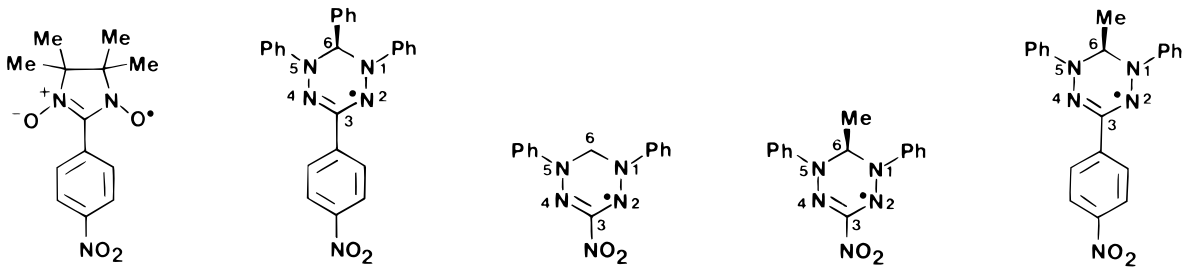

1 **2** **3** **4** **5**

detail. Furthermore, it was mentioned[8] that **2** might perhaps undergo structural phase transitions near room temperature and about 100 K. This point should also be clarified.

The aim of this work was to extend the studies to verdazyls with a substitution pattern comparable to that of **1** and **2,** to verdazyls with strong electron acceptor groups in the 3-position, e.g., 3-nitro-1,5-diphenylverdazyl (**3**), and to related verdazyls with a methyl group in the 6-position, 6-methyl-3-nitro-1,5-diphenylverdazyl (**4**) and 6-methyl-3-(4-nitrophenyl)-1,5-diphenylverdazyl (**5**). The methyl group in the 6-position could have a similar effect on the crystal packing as the 6-phenyl substituent in **2**.

2. Experimental Section

2.1. Syntheses. 3-(4-Nitrophenyl)-1,5,6-triphenylverdazyl (**2**)[8] and 3-nitro-1,5-diphenylverdazyl (**3**)[10] were prepared as described in the literature.

6-Methyl-3-nitro-1,5-diphenylverdazyl (4). To a stirred solution of 3-nitro-1,5-diphenylformazan[11] (4.05 g, 15 mmol) in dimethyl sulfoxide (50 mL) at 20 °C, potassium *tert*-butoxide (95%, 3.48 g, 30 mmol) and iodoethane (4.70 g, 2.4 mL, 30 mmol) were added in portions, and stirring at ambient temperature was continued for 8 h. Then the mixture was poured into water (500 mL), and the products were extracted with diethyl ether (3 × 250 mL). The combined extracts were washed with water, dried ($MgSO_4$), and evaporated. The residue was chromatographed on aluminum oxide (Brockmann) using toluene as eluent to give as a first fraction 1-ethyl-1,2,3,4-tetrahydro-3-methyl-2,4-diphenyl-6-nitro-*s*-tetrazine (1.46 g, 30%; DC Micro Cards Polygram ALOX N/UV$_{254}$, Macherey-Nagel, R_f = 0.69, toluene) as orange prisms from ethanol, mp 104 °C. ^{1}H NMR (Bruker AM 360 MHz, [D$_6$]DMSO, 305 K): δ = 1.21 (t, ^3J = 7.0 Hz, 3H, CH_2CH_3), 1.55 (d, ^3J = 6.4 Hz, 3H, $CHCH_3$), 3.43 (dq, $^2J \approx 14$ Hz, $^3J \approx 7$ Hz, 1H, CH_2CH_3), 3.76 (dq, $^2J \approx 14$ Hz, $^3J \approx 7$ Hz, 1H, CH_2CH_3), 6.49 (q, ^3J = 6.4 Hz, 1H, $CHCH_3$), 6.91−6.96 (m, 2H, phenyl H), 7.21−7.32 (m, 8H, phenyl H). MS: *m*/*z* 325 ($M^{\bullet+}$, 10%), 204 (16%), 120 (12%), 119 (100%), 104 (28%), 93 (12%), 91 (18%), 78 (10%), 77 (88%). Anal. Calcd for $C_{17}H_{19}N_5O_2$: C, 62.76; H, 5.89; N, 21.52. Found: C, 62.97; H, 6.11; N, 21.42. Further elution with toluene yielded starting material 3-nitro-1,5-diphenylformazan (1.10 g, 24%; R_f = 0.58, toluene) and finally compound **4** (380 mg, 8.5%; R_f = 0.33, toluene) as black metallescent crystals from ethanol, mp 161 °C (dec). MS: *m*/*z* 297 (15%), 296 (M^+, 78%), 131 (6%), 120 (14%), 119 (98%), 105 (28%), 104 (72%), 78 (6%). Anal. Calcd for $C_{15}H_{14}N_5O_2$: C, 60.81; H, 4.76; N, 23.63. Found: C, 60.98; H, 4.85; N, 23.34.

6-Methyl-3-(4-nitrophenyl)-1,5-diphenylverdazyl (5). A mixture of 3-(4-nitrophenyl)-1,5-diphenylformazan[12] (2.07 g, 6 mmol), barium oxide (6 g), iodoethane (9.36 g, 5 mL, 60 mmol), and water (0.5 mL) in dimethylformamide (80 mL) was stirred at ambient temperature for 1 d. The mixture was filtered, and to the filtrate, methanol and water were added. The precipitated brown product was collected and chromatographed on aluminum oxide (Brockmann) using toluene as eluent to give compound **5** (1.63 g, 73%) as black-brown crystals from tetrahydrofuran−methanol, mp 230−231 °C (dec). MS: *m*/*z* 373 (9%), 372 (M^+, 57%), 119 (10%), 104 (36%), 77 (100%). Anal. Calcd for $C_{21}H_{18}N_5O_2$: C, 67.73; H, 4.87; N, 18.81. Found: C, 67.89; H, 4.95; N, 18.73.

2.2. Crystal Data and Structure Determination. For **2** and **4** the diffraction data were collected at 22 °C on an Enraf-Nonius CAD-4 four-circle diffractometer, using graphite-monochromated Mo Kα radiation (λ = 0.710 69 Å, $\omega-2\theta$ scanning technique). Lattice parameters were determined from a least-squares fit using 30 reflections (θ range: 10−14°). The structures were solved by direct methods (programs used: Enraf-Nonius,[13] SIR 92[14]) and were refined by full-matrix least-squares minimizing $\sum w(\Delta F)^2$ with the weighting scheme $w = [\sigma(F)^2 + (0.03F_0)^2]^{-1}$. Hydrogen atoms were refined with isotropic temperature factors and all other atoms with anisotropic temperature factors.

The lattice parameters for **3** were obtained at 25 °C on a Rigaku AFC5R four-circle diffractometer by least-squares refinement on diffractometer angles for 25 automatically centered reflections in the range 18.0° ≤ 2θ ≤ 22.3°, using graphite-monochromated Mo Kα radiation (λ = 0.71069 Å) from a 12 kW type rotating-anode generator equipped with a fine-focus anode. The intensity data were collected on the same diffractometer and at the same temperature. The reflections with 45.0° ≤ 2θ could not be collected because of very weak intensities due to the thickness of the sample crystal (0.40 × 0.35 × 0.02 mm^3) and the low quality of the crystal. The $\omega-2\theta$ scan mode with a scan rate of 16° min^{-1} (in ω) was applied for 1893 unique reflections, giving 621 with $I \geq 3.0\sigma(I)$, which were labeled observed and used in the structure refinement. Two rescans were applied for weak reflections. Corrections were made for the Lorentz and polarization factors. Three standard reflections monitored at every 150 reflections showed an intensity deterioration by 4.50% of the initial value. The falling-off of the intensities with the elapse of time was corrected based on the linear decay in the standard reflections. The stucture was solved by direct methods (program used: TEXSAN[15]) and refined by the similar full-matrix least squares procedure with the weighting scheme $\omega = 1/[\sigma^2(F_0)]$. The positions of the hydrogen atoms were idealized (C−H, 0.95 Å), assigned to isotropic thermal parameters B(H) = 1.2B_{eq}(C), and allowed to ride on their parent carbons.

The crystallographic data, the methods of structure solution, and the parameters of the structure refinement of **2**−**4** are given in Table 1.[16]

2.3. Measurements of Magnetic Susceptibility. The paramagnetic susceptibility measurements were carried out with a Shimadzu MB-2 type magnetic torsion balance in the

TABLE 1: Crystallographic Data and Refinement Parameters of 2−4

	2	**3**	**4**
chemical formula	$C_{26}H_{20}N_5O_2$	$C_{14}H_{12}N_5O_2$	$C_{15}H_{14}N_5O_2$
formula weight	434.5	282.3	296.3
crystallized from	toluene	benzene	ethanol
crystal size/mm^3	0.30 × 0.15 × 0.07	0.40 × 0.35 × 0.02	0.3 × 0.3 × 0.2
crystal system	triclinic	monoclinic	monoclinic
space group	$P\bar{1}$ (no. 2)	$P2_1/n$ (no. 14)	$P2_1/n$ (no. 14)
a/Å	6.596(2)	3.9994(6)	11.657(5)
b/Å	12.755(4)	14.926(2)	19.272(7)
c/Å	13.160(4)	22.028(3)	13.043(5)
α/(deg)	87.24(2)		
β/(deg)	84.16(2)	94.55(1)	97.39(2)
γ/(deg)	83.90(2)		
Z	2	4	8
V/Å^3	1094(1)	1310.8(3)	2906(3)
F_{000}/e	454	588	1240
D_x/g cm^{-3}	1.316	1.430	1.356
μ/mm^{-1} (Mo Kα)	0.081	0.094	0.089
measured reflections	4291	1893	5932
$(\sin\theta/\lambda$ Å$^{-1})_{max}$	0.62	0.54	0.63
observed reflections [$I \geq 3.0\sigma(I)$]	2096	621	2367
refinement R/R_w	0.048/0.054	0.050/0.044	0.047/0.039
$(\Delta/\sigma)_{max}$	0.08	0.00	0.03
$(\Delta\rho$/e Å$^{-3})_{max}$	0.21(5)	0.19(5)	0.34(4)
structure solution	direct methods (SIR)	direct methods (MITHRIL)	direct methods (SIR)

TABLE 2: Selected Structural Data of 1,3,5-Triphenylverdazyl (6)[18] and of the Verdazyls 2−4

	6	**2**	**3**	**4**[a]
N1−N2/Å[b]	1.351(3)	1.355(3)	1.358(8)	1.349(6)
N2−C3/Å[c]	1.338(1)	1.335(8)	1.32(1)	1.321(6)
N1−C6/Å[d]	1.443(3)	1.461(8)	1.457(9)	1.464(4)
N1−N2−C3/(deg)[e]	114.4(2)	114.4(9)	111.6(7)	112.2(2)
N2−C3−N4/(deg)	126.8	127.4(3)	132.7(8)	131.7(3)
N4−N5−C6/(deg)[f]	117.8(4)	117.5(8)	116.8(7)	118.4(5)
N1−C6−N5/(deg)	106.1	104.8(3)	106.8(6)	105.8(2)
C3/Å[g]	+0.099	+0.093(4)	+0.110(7)	+0.093(3)
C6/Å[g]	+0.590	+0.621(4)	+0.603(7)	0.582(5)
interplanar angle/(deg)[h]	10	10	12	10
Interplanar angle/(deg)[i]	43	44	44	41

[a] Mean values of molecules A and B; see text. [b] Mean value of N1−N2 and N4−N5 bond lengths. [c] Mean value of N2−C3 and C3−N4 bond lengths. [d] Mean value of N1−C6 and N5−C6 bond lengths. [e] Mean value of N1−N2−C3 and C3−N4−N5 angles. [f] Mean value of N4−N5−C6 and N2−N1−C6 angles. [g] Deviation out of the N1−N2−N4−N5 plane. [h] Interplanar angle between the N1−N2−N4−N5 and N2−C3−N4 planes. [i] Interplanar angle between the N1−N2−N4−N5 and N1−C6−N5 planes.

temperature range 77−300 K and with a SQUID magnetometer (HOKUSAN HSM 2000) in the temperature range 4.2−100 K. For verdazyl **2**, the ac susceptibility (χ_{ac}) measurements were performed in the temperature range of 1.67−100 K using the Lake Shore 7110 ac susceptometer at $f = 125$ Hz. Furthermore, for this compound ac susceptibilities were also measured in the temperature range 0.67−5.8 K by use of the Linear Research Inc. LR-700 ac resistance bridge at $f = 15.9$ Hz. The susceptibilities were corrected for the diamagnetic contributions of $\chi_{dia} = -0.241 \times 10^{-3}$ (**2**), -0.139×10^{-3} (**3**), -0.155×10^{-3} (**4**), and -0.204×10^{-3} emu/mol (**5**) calculated by Pascal's method.

2.4. Measurement of Heat Capacity. Measurements of heat capacity, C_p, were performed for **2** and **3** above 0.73 K, using the usual type of adiabatic calorimeter described previously in detail.[17] The measurements were performed on 0.3179 g (**2**) and 0.5168 g (**3**) powder samples and were corrected for the heat capacity of the addenda.

3. Results

3.1. Crystal Structures. For **3** and **4** the crystal structure, an essential prerequisite for the understanding of specific molecular properties in the solid state, could be determined. In addition, a repeated structure analysis of **2** led to a better refinement. Our attempts, however, to determine the crystal structure of **5** have as yet been unsuccessful because of the inadequate quality of its crystals. Pertinent bond lengths and bond angles of **2**−**4** are given in Table 2. The data of the central hydrazidinyl moiety N1−N2−C3−N4−N5 are very similar to those of 1,3,5-triphenylverdazyl[18] and other 1,3,5-triarylverdazyls.[19−23] As in these compounds the four nitrogens of the verdazyl ring in **2**−**4** are nearly planar and the verdazyl ring has an unsymmetrical boat conformation, with both C3 and C6 being out of the nitrogen plane on the same side. C3 is displaced by only +0.1 Å, while C6 is displaced by +0.6 Å. Corresponding to these displacements, the interplanar angle between the N1−N2−N3−N4 and N2−C3−N4 planes is about 10° and between the N1−N2−N3−N4 and N1−C6−N5 planes about 43° (Table 2).

In the 3-(4-nitrophenyl)-1,5,6-triphenylverdazyl (**2**) the bulky 6-phenyl substituent apparently prevents an upright columnar stacking of the verdazyls. As shown in Figure 1, the molecules are mutually shifted by about 5.5 Å along the N1···N2 direction and build up a stairlike chain structure. Furthermore, a closer inspection (Figure 2) reveals that the molecules are also laterally shifted with respect to each other by about 0.6 Å. As a consequence, the central verdazyl ring overlaps only partially with the adjacent coplanar 3-(4-nitrophenyl) substituent. The shortest intermolecular contacts are found between O34a and C31^i [$d_1 = 3.372(5)$ Å], O34a and C3^i [$d_2 = 3.381(5)$ Å], C35

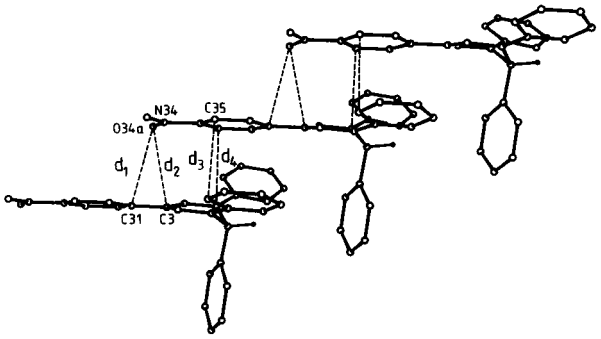

Figure 1. Crystal packing of 3-(4-nitrophenyl)-1,5,6-triphenylverdazyl (**2**) in a side view showing the stair pattern and the intermolecular overlap between adjacent molecules. Shortest intermolecular contacts between the adjacent verdazyl ring and the 3(4-nitrophenyl) substituent are the following: O34a···C31^{i}, d_1 = 3.372(5) Å; O34a···C3^{i}, d_2 = 3.381(5) Å; C35···C16^{i}, d_3 = 3.369(6) Å; C33···N5^{i}, d_4 = 3.398(6) Å [symmetry code i, 1 + *x*, *y*, *z*].

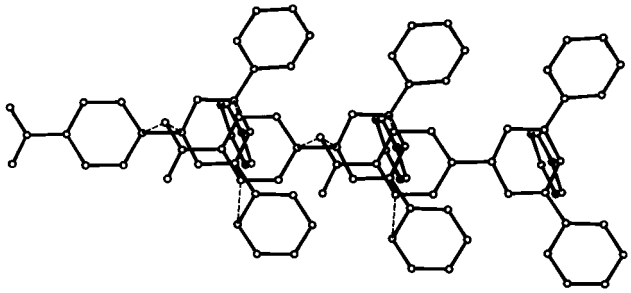

Figure 2. View perpendicular to the verdazyl N1−N2−N4−N5 plane of **2** showing the side shift of the chain.

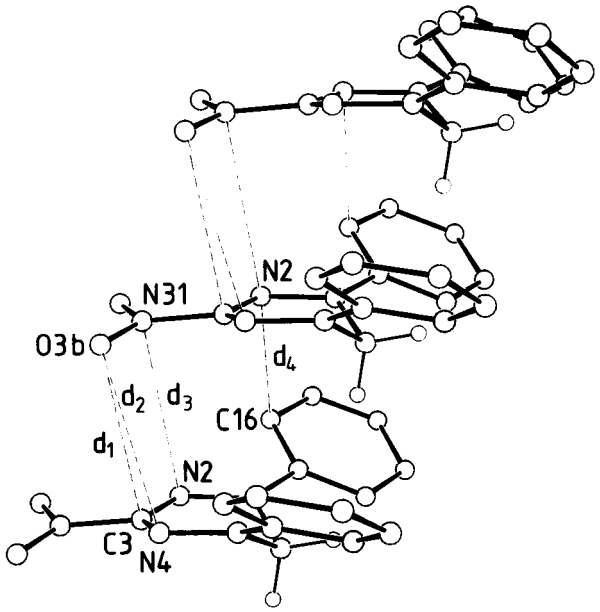

Figure 3. Crystal packing of 3-nitro-1,5-diphenylverdazyl (**3**) in a side view showing the stair pattern and the intermolecular overlap between adjacent molecules. The shortest intermolecular contacts within the stair pattern are the following: O3b···C3^{i}, d_1= 3.44(1) Å; O3b···N4^{i}, d_2 = 3.42(1) Å; N31···N2^{i}, d_3 = 3.57(1) Å; N2···C16^{i}, d_4 = 3.27(1) Å [symmetry code i, + *x*, *y*, *z*]

and C16^{i} [d_3 = 3.369(6) Å], and C33 and N5^{i} [d_4 = 3.398(6) Å] [symmetry code i, 1 + *x*, *y*, *z*] (Figure 1). The angle between the stacking *a* axis and the normal to the nitrogen planes is 55°.

Similar to the crystal structure of **2**, the 3-nitro-1,5-diphenylverdazyl (**3**) is also stacked in a stairlike pattern along the *a* axis. The mutual shift along the N1···N2 direction, however, is significantly shorter, about 1.4 Å, as is the lateral shift, about 0.3 Å. In contrast to compound **2**, in the crystal structure of **3** the adjacent verdazyls show some overlap of the central verdazyl rings. The shortest intermolecular contacts are found between O3b and C3^{i} [d_1 = 3.44(1) Å], O3b and N4^{i} [d_2 = 3.42(1) Å], N31 and N2^{i} [d_3 = 3.57(1) Å], and N2 and C16^{i} [d_4 = 3.27(1) Å] [symmetry code i, 1 + *x*, *y*, *z*] (Figure 3). The angle between the stacking *a* axis and the normal to the nitrogen planes is found to be 23°.

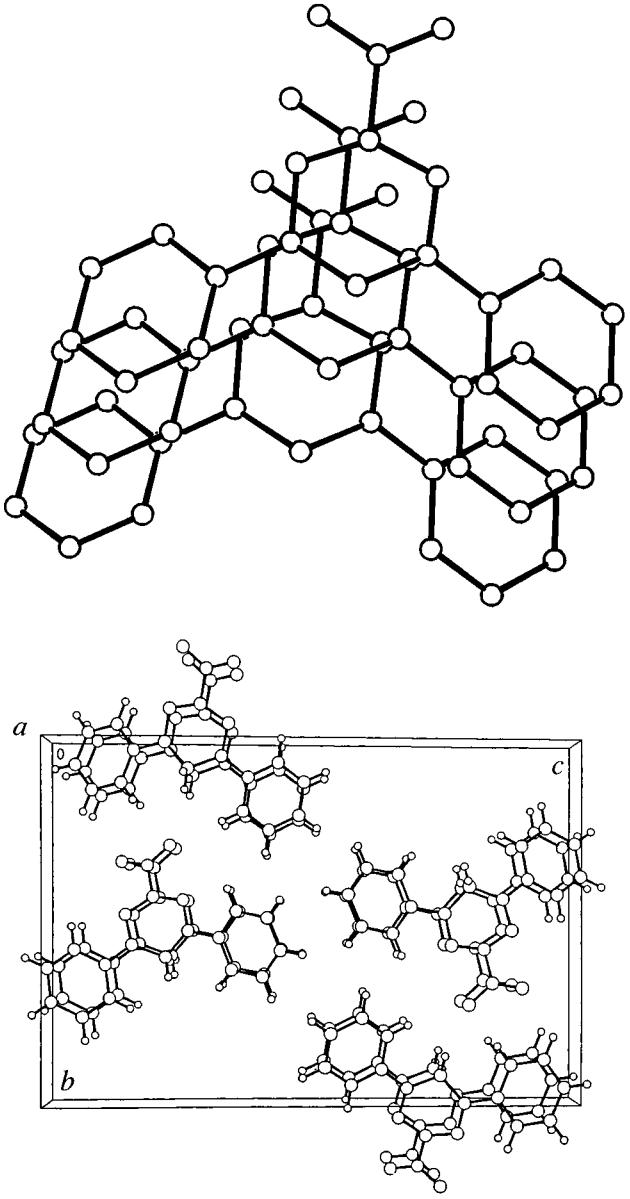

Figure 4. View perpendicular to the verdazyl N1−N2−N4−N5 plane of **3** showing the side shift of the chain (top) and crystal structure of **3** viewed along the direction perpendicular to the *bc* plane (bottom).

Like the 6-phenyl substituent in **2** the 6-methyl group of the 6-methyl-3-nitro-1,5-diphenylverdazyl (**4**) is almost perpendicularly arranged with respect to the verdazyl nitrogen plane (Figure 5). The displacement of C6 from that plane necessarily leads to an opposite displacement of C11 and C51 to retain planarity about N1 and N5. Owing to their steric requirements the N-phenyl groups are distorted in a mutual antipropeller fashion. As a whole, the conformational arrangement of the central verdazyl ring in **4** corresponds to those of **2** and **3**. In the unit cell of **4** there are eight verdazyls arranged in two groups of nonequivalent molecules A and B, which with regard to their molecular details show no significant differences. The crystal

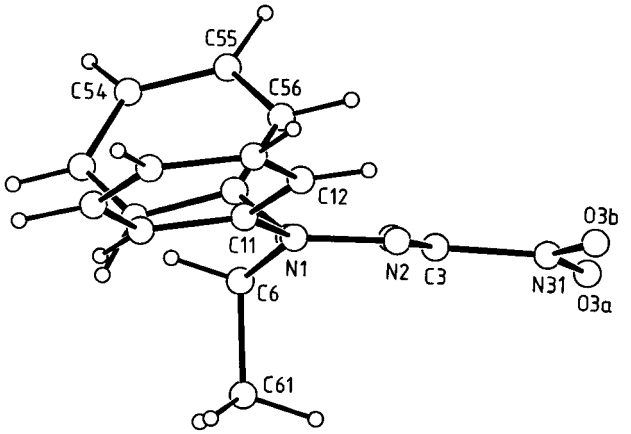

Figure 5. View of 6-methyl-3-nitro-1,5-diphenylverdazyl (**4**) with the atom labeling scheme.

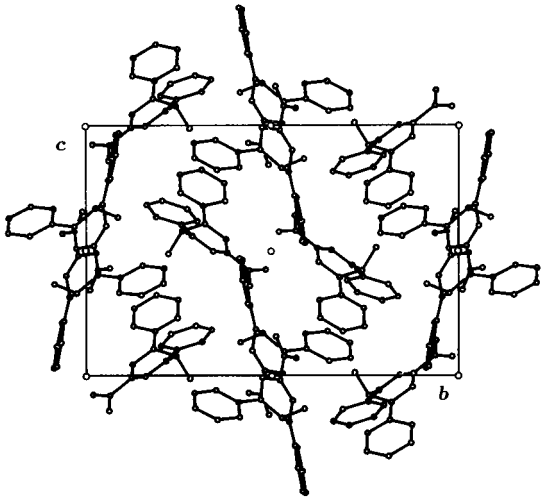

Figure 6. Packing diagram of **4** projected down the *a* axis.

packing of **4**, however, deviates completely from those of **2** and **3**. As Figure 6 illustrates, there is no distinct order or stacking.

3.2. Magnetic Properties of 3-(4-Nitrophenyl)-1,5,6-triphenylverdazyl (2). The ac susceptibility, χ_{ac}, of **2** follows the Curie−Weiss law with a positive Weiss constant, θ, of +3.1 ± 0.2 K, indicating dominant ferromagnetic exchange interaction between neighboring verdazyl molecules, as reported by Allemand et al.[8] At lower temperatures (<20 K), however, the inverse susceptiblity versus T is no longer linear, as shown in Figure 7. The low-temperature χ_{ac} shows a sharp peak at T_{max} = 1.16 K and decreases toward 0 K with its magnitude of about $^2/_3$ of the peak value of χ_{ac} at 1.16 K, as in ordinary powder crystal susceptibilities of antiferromagnets. The result suggests that **2** undergoes an antiferromagnetic transition at T_N = 1.16 K.

As described in the later thermal analysis, **2** has characteristics of a quasi-one-dimensional (quasi-1D) ferromagnet above T_N. Therefore, the low-temperature behavior of the χ_{ac} of **2** was analyzed on the basis of the quasi-1D ferromagnetic Heisenberg model with the Hamiltonian as

$$H = -2J\sum_{i=1} S_i S_{i+1} - g\mu_B H\sum_{i=1} S_i^z - 2J'\sum_{\langle ij \rangle} S_i S_j \qquad (1)$$

where J and J' are the intra- and interchain exchange integrals, respectively, and H is the applied field.

As the first approximation, we consider the case for $J' = 0$ for which χ_{ac} in the paramagnetic state of **2** may be described.

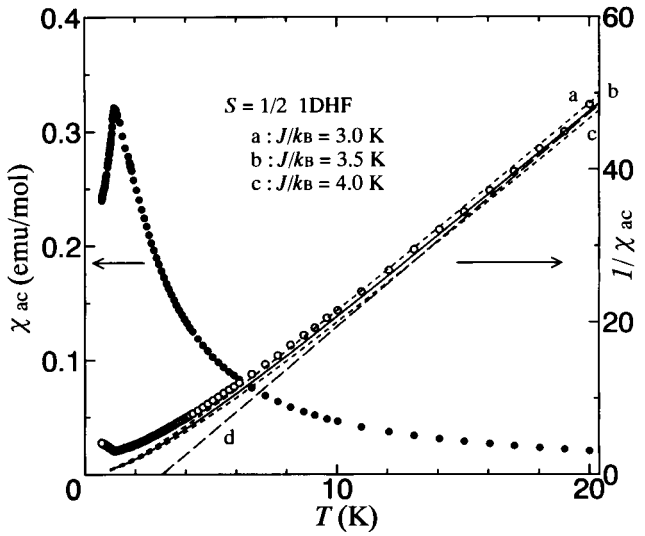

Figure 7. Molar and inverse molar magnetic susceptibilities χ_{ac} and $1/\chi_{ac}$ of 3-(4-nitrophenyl)-1,5,6-triphenylverdazyl (**2**) at low temperatures. Above 6 K, the observed values (open circles) obey the theoretical results for the 1D isotropic Heisenberg ferromagnet (1DHF, eq 2)[24] with $2J/k_B = +7.0 \pm 1.0$ K indicated by the solid line b: $J/k_B = 3.5$ K. The dotted lines a and c represent the theoretical values of the susceptibilities calculated for $J/k_B = 3.0$ and 4.0 K, respectively. The broken line d represents the Curie−Weiss law with $\theta = +3.1$ K.

In such a case, the susceptibility of a 1D ferromagnet with $S = {}^1/_2$, χ_{1D}, is given by

$$\chi_{1D} = \frac{Ng^2\mu_B^2}{4k_BT}\left\{1 + \left(\frac{J}{k_BT}\right)^a\right\} \qquad (2)$$

with $a = 1$ for $k_BT/J > 1$.[24] In fact, our data are well reproduced by eq 2 with $2J/k_B = +7.0 \pm 1.0$ K and $g = 2.00$ as shown in Figure 7, deviating from the Curie−Weiss behavior.

At lower temperatures, we have to consider the effect from the interchain interaction (J') that triggers the three-dimensional ordering at T_N. From the mean field theory,[25] which gives the relation $kT_N \cong 2S^2(|zJ'|J)^{1/2}$ (z, the number of neighboring chains), $|J'/J|$ is estimated to be ≅0.11 with T_N = 1.16 K and J/k_B = 3.5 K, assuming $z = 4$. The Oguchi theory[26] estimates $|J'/J| \cong 0.04$. The low-temperature deviation of χ_{ac} of **2** from eq 2 is mainly due to this effect of the $|J'/J| \cong 0.04-0.11$.

Figure 8 shows the experimental results of heat capacity, C_p. A distinct peak that corresponds to a three-dimensional magnetic phase transition is detected at T_N = 1.10 K, and a flat plateau follows in the higher temperatures above T_N. For extracting the magnetic heat capacity C_m from C_p, we assume that the lattice heat capacity C_l is expressed as the Debye function, which depends on the Debye temperature θ_D and the effective number of oscillating atomic units r in a unit cell ($r = 1$ for the simple cubic lattice composed of one kind of atom, for example). At low temperatures it usually gives a T^3 dependence. On the other hand, the magnetic entropy $S_m(T)$ is expressed with C_m as

$$S_m(T) = \int_0^T (C_m/T)\,dT \qquad (3)$$

which is eventually equal to $Nk_B \ln(2S + 1)$ at $T \rightarrow \infty$, or $S_m(\infty) = Nk_B \ln 2$ for $S = {}^1/_2$. Here, the value of C_l is so determined, since the magnetic heat capacity C_m ($=C_p - C_l$) gives the value $S_m(\infty)$ with the use of eq 3 for adjusting the parameters θ_D and r. In this procedure, C_p is taken from the experimental results for 0.73 K < T < 13 K as seen in Figure 8. For T < 0.73 K, C_m is estimated to be $C_m = bT^3$ under the assumption of the three-dimensional spin wave theory, and for T > 13 K, C_m =

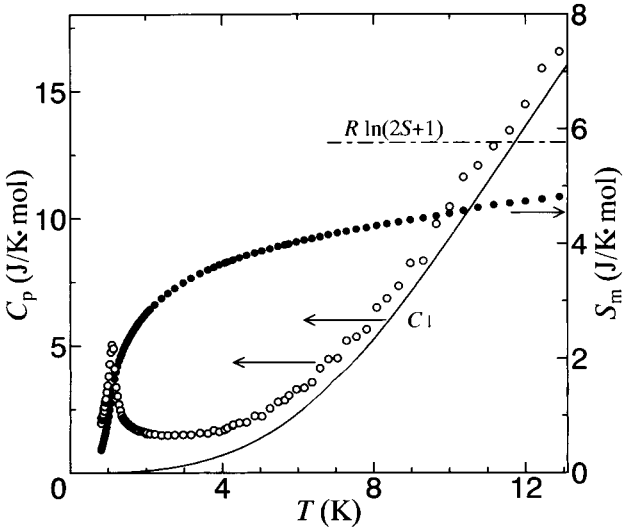

Figure 8. Heat capacity C_p (open circles) of **2** in the temperature range 0.73−13 K. The solid line is the estimated lattice contribution C_l. Closed circles are the magnetic entropy S_m.

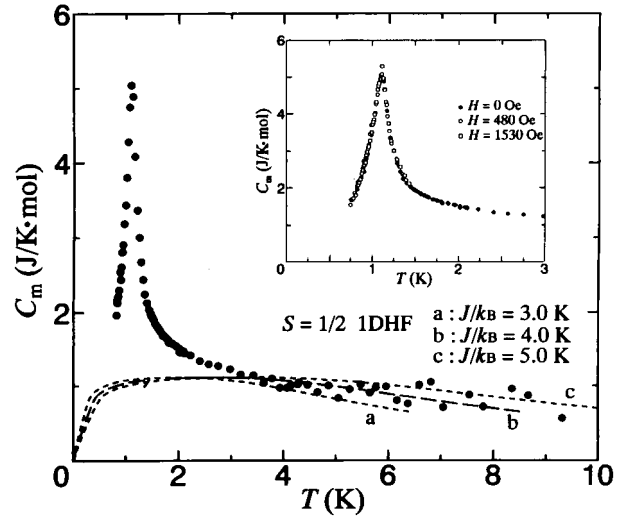

Figure 9. Temperature dependence of the magnetic heat capacity C_m of **2** (closed circles). Theoretical results for the isotropic 1D Heisenberg ferromagnet (1DHF)[24] are drawn for $2J/k_B = +6.0$, 8.0, and 10.0 K. The inset shows the field dependence of the magnetic heat capacity C_m.

cT^{-2} as in ordinary paramagnetic state. In Figure 8, the best Debye function (C_l) is illustrated for $\theta_D = 71$ K and $r = 2$. The value of θ_D of this radical crystal is smaller compared with those of inorganic metallic substances, implying the mechanically soft properties of organic compounds. The temperature dependence of $S_m(T)$ is also given in Figure 8, which seems to approach the limiting value $S_m(\infty)$ for $T \gg 13$ K.

The intrinsic magnetic heat capacity, C_m, of **2** is shown in Figure 9. It is noted that the plateau of the heat capacity is reproduced by the theory for the 1D Heisenberg ferromagnet[24] with $2J/k_B = 8.0 \pm 2.0$ K (see Figure 9) as in the case of the magnetic susceptibility ($2J/k_B = 7.0 \pm 1.0$ K). The sharp heat capacity peak is stable even in external fields up to 1.53 kOe, as seen in the inset of the Figure 9. This field dependence of the peak makes a good contrast to the sensitive field dependence in the β-phase of 4,5-dihydro-4,4,5,5-tetramethyl-2-(4-nitrophenyl)-1*H*-imidazol-1-yloxy 3-oxide (**1**), where the peak becomes a round maximum with about a half height of the peak even in a field of 0.15 kOe.[3c] Rather, the behavior of **2** in the fields resembles the case of the antiferromagnetic γ phase of **1**.[3c]

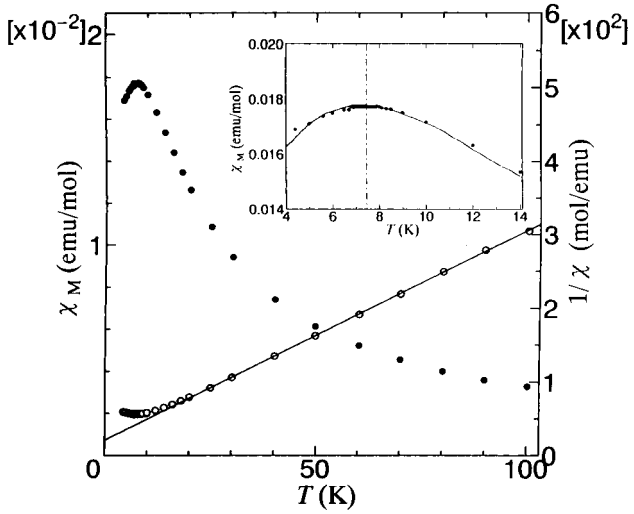

Figure 10. Molar and inverse molar magnetic susceptibilities χ_M and $1/\chi_M$ of 3-nitro-1,5-diphenylverdazyl (**3**). The inset shows the magnetic susceptibility (solid line) of **3** calculated for the value of $2J/k_B = -11.6$ K in the temperature range 4−14 K.

In zero field and in the paramagnetic state, C_m of **2** keeps the values comparable to $C_m(\max) = 0.134R = 1.12$ J/(mol K) above 3 K, which is a characteristic feature of the isotropic 1D Heisenberg ferromagnet.[24] Further evidence for the one-dimensional interaction in **2** is provided by its crystal structure determination. As shown in Figures 1 and 2, the verdazyls **2** are stacked along the *a* axis, building up a stairlike chain structure.

As a conclusion, **2** is an antiferromagnet with a Neel temperature of $T_N = 1.10 \pm 0.03$ K and behaves as a quasi-1D ferromagnet with the intrachain exchange interaction of $2J/k_B = 7.0 \pm 1.0$ K above the transition temperature T_N. Experimentally, there are no indications of any structural phase transitions between 10 K and room temperature.

Recently, the magnetic properties of organic radical crystals have been studied extensively, generally indicating the antiferromagnetic intermolecular interaction in these radical crystals. However, as far as we know, the examples of real antiferromagnets that show the antiferromagnetic long-range order are very limited. Furthermore, they are nitroxides[27−30] and the nitronyl nitroxide **1**,[3c] except for the case of the 1,3-bisdiphenylene-2-(4-chlorophenyl) allyl radical, which is known as an example of the first antiferromagnet.[31] For this carbon-centered radical the highest Neel temperature $T_N = 3.25$ K has been observed.[31] The Neel temperature of **2**, $T_N = 1.10$ K, is the second highest one of genuine organic antiferromagnets.

3.3. Magnetic Properties of 3-Nitro-1,5-diphenylverdazyl (3). The magnetic susceptibility, χ_M, obtained for the verdazyl **3** is shown in Figure 10 as a function of temperature. The susceptibility of **3** follows the Curie−Weiss law with a Curie constant of 0.352 K emu/mol and a Weiss constant of -7.3 ± 0.5 K in the temperature region between 20 and 300 K. The susceptibility shows a broad maximum at $T_{max} = 7.4 \pm 0.2$ K. After passing through the maximum, the susceptibility falls off slowly till 4.2 K and a finite susceptibility at 0 K seems to be left, as seen in Figure 10. The result suggests that the 1D antiferromagnetic Heisenberg model (that is, nonalternating antiferromagnetic Heisenberg linear chain model) is appropriate for describing the magnetic system.[24]

The theoretical curve calculated from the 1D antiferromagnetic Heisenberg model gives an excellent fit to the observed one, as shown in Figure 10.[24] The exchange integral ($2J/k_B$) was estimated to be -11.6 K, using the relation $kT_{max}/|J| = 1.282$.

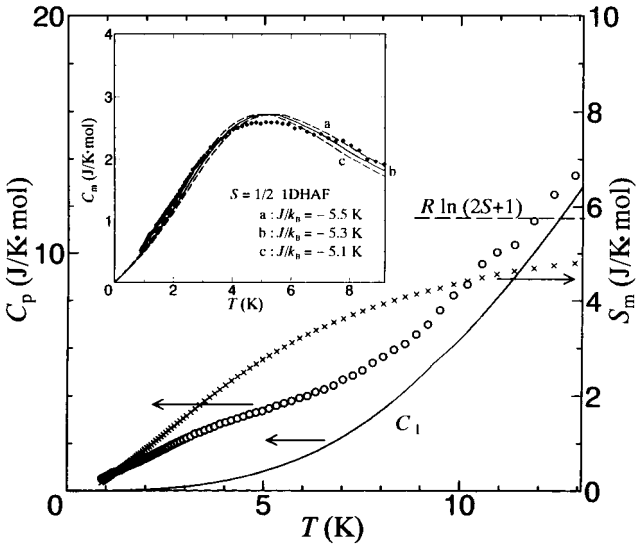

Figure 11. Heat capacity C_p of **3** in the temperature range 0.89−16 K. The solid line gives the estimated lattice contribution C_l. The inset shows the magnetic heat capacity C_m of **3**. The dashed line is the result of the theoretical calculation (see text).

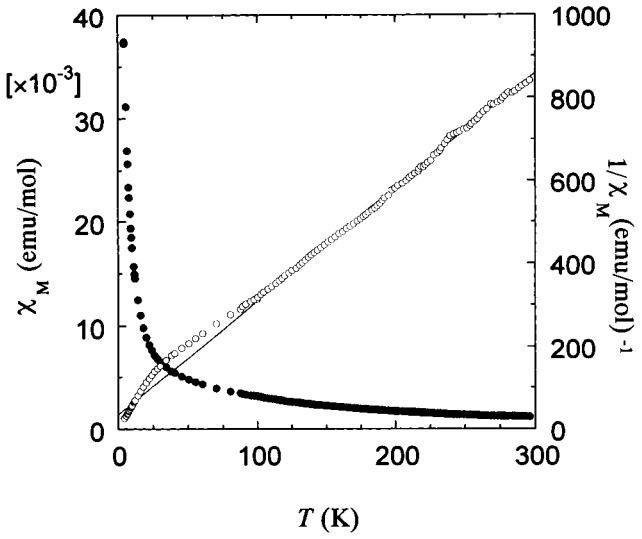

Figure 12. Temperature dependence of the molar and inverse molar magnetic susceptibilities χ_M and $1/\chi_M$ of 6-methyl-3-nitro-1,5-diphenylverdazyl (**4**).

The heat capacity, C_p, of **3** was measured under zero external field in the temperature range 0.89−16 K. The results obtained are shown in Figure 11. The main contributions to the heat capacity come from the lattice and the magnetic systems. The lattice heat capacity, C_l, was estimated as performed for **2**. The Debye function is determined so that the total magnetic entropy $S_m(\infty)$ equals $Nk_B \ln 2$ in **3**. The Debye temperature and effective number of oscillators obtained are $\theta_D = 96$ K and $r = 3$, respectively. The temperature dependences of the magnetic entropy, S_m, and the lattice heat capacity, C_l, are shown in Figure 11. The magnetic heat capacity curve for $0.89 < T < 9$ K is obtained by subtracting the value of $C_l(T)$ from the total C_p, and this is plotted in the inset of Figure 11.

Verdazyl **3** has the characteristics of a 1D Heisenberg antiferromagnet with $S = {}^1/_2$, as obtained from the result of the magnetic susceptibility measurement. In fact, as shown in the inset of Figure 11, the theoretical curve fits the experimental data with $2J/k_B = -10.6 \pm 0.4$ K. The value of $2J/k_B$ (−10.6 K) shows good accordance with that (−11.6 K) obtained from the static magnetic susceptibility measurement. The result of the present experiment shows that the Neel temperature T_N of **3** under zero external field is lower than 0.7 K, suggesting strong one-dimensionality of the spin correlation in **3**.[32]

As described in a previous section, the crystal structure of verdazyl **3** shows a particular one-dimensional arrangement of the verdazyl moieties (Figures 3 and 4). The molecules of **3** are packed in columns along the *a* axis. Within the array the verdazyl ring and the verdazyl ring of adjacent verdazyl molecules lie parallel to each other, and the short intermolecular contacts N4···N5^i and N2···N1^i are 3.69 and 3.73 Å, respectively [symmetry code i, $1 + x, y, z$].

In view of the crystal structure of **3**, the $S = {}^1/_2$ 1D antiferromagnetic Heisenberg linear chain model[24] appears appropriate for describing the magnetic system. The strong one-dimensionality of the spin correlation in **3** will be due to the isolation between the columns (see Figure 4, bottom).

3.4. Magnetic Properties of 6-Methyl-3-nitro-1,5-diphenylverdazyl (4). The molar susceptibility, χ_M, of **4** follows the Curie−Weiss law with a Curie constant of 0.372 K emu/mol and a Weiss constant of -18 ± 2 K in the temperature region between 100 and 300 K, as shown in Figure 12. The radical concentration calculated from the above Curie constant is 99% for **4**. Below 100 K the plot $1/\chi_M$ versus T is no longer linear and deviates upward. This suggests an antiferromagnetic intermolecular interaction in **4** at low temperature. However, below about 25 K the value of $1/\chi_M$ decreases and approaches zero at $T = 0$. The increase in susceptibility at low temperature may be attributable to isolated monoradicals and/or broken-chain effects.[24] However, the residual paramagnetic radical concentration, calculated from the susceptibility at 4.2 K and assuming validity of the Curie law, is about 10%. The susceptibility of independently prepared crystalline **4** samples also showed quite a similar behavior, suggesting that this increase in the susceptibility is not due to a monoradical impurity but to an intrinsic property of **4**. As Figure 6 illustrates, the crystal packing of **4** shows no distinct order and is quite different from those of **2** and **3**, which are stacked in a stairlike chain pattern along the *a* axis and show 1D magnetic behavior. However, the details of the magnetic property of **4** are not clear at present.

3.5. Magnetic Properties of 6-Methyl-3-(4-nitrophenyl)-1,5-diphenylverdazyl (5). The magnetic susceptibility obtained for **5** is shown in Figure 13 as a function of temperature. When the temperature is lowered from 300 K, χ_M increases gradually and reaches a broad maximum at $T_{max} = 69 \pm 2$ K. After passing through the maximum, χ_M falls off gradually to 14 K. Below this temperature, χ_M increases again as the temperature is lowered. This increase of the susceptibility at low temperature is probably due to isolated monoradicals that are randomly located in the lattice. The residual paramagnetic radical concentration, calculated from the susceptibility at 4.2 K and assuming validity of the Curie law, is only 1.2%. The low-temperature paramagnetic impurity curve is extrapolated to higher temperatures and subtracted from the experimental one. In Figure 13, the corrected susceptibility−temperature data (closed circles) for **5** are given along with the theoretical curves for the alternating antiferromagnetic Heisenberg linear chain model with $\alpha = 0.2$, 0.4, and 0.6.[33] α ($=J_2/J_1$) is a parameter that conveniently indicates the degree of alternation, and $\alpha = 1$ corresponds to the uniform limit, that is, a nonalternating antiferromagnetc chain. The "best fit" $a = 0.4$ curve corresponds to $2J_1/k_B = -113$ K and $2J_2/k_B = -45$ K.

The antiferromagnetic exchange interaction ($2|J_1|/k = 113$ K) observed in solid **5** is very large. As far as we know, this is the largest value of $|2J|$ found for verdazyl type free radical solids.[34−37] The result suggests that the molecules of **5** are packed in columns, showing 1D magnetic properties, and the

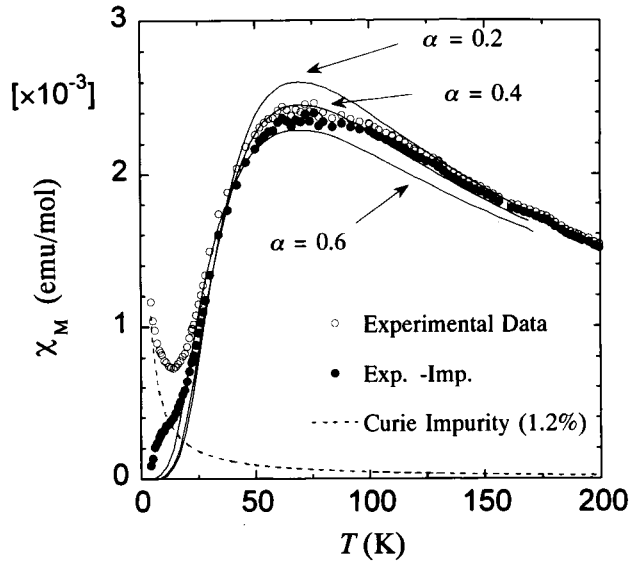

Figure 13. Molar magnetic susceptibility χ_M of 6-methyl-3-(4-nitrophenyl)-1,5-diphenylverdazyl (**5**). The open circles are the experimental points. The broken line is calculated for 1.2% of a monoradical impurity following the Curie law. The closed circles give the difference between experimental and impurity curves. The solid lines are theoretical fits corresponding to α values of 0.2, 0.4, and 0.6.

verdazyl rings with high-spin density overlap each other with comparatively short intermolecular distances in the crystal. However, the details are not clear at present because our attempts to determine the crystal structure of **5** have as yet been unsuccessful because of the inadequate quality of the crystals.

Acknowledgment. We are grateful to Mr. N. Wada and Mr. S. Kawasaki for their kind help in measuring the susceptibility of these radical solids. This work was partly supported by a Grant-in-Aid for Scientific Research on priority area Molecular Magnetism (Area No. 228/04242104) from the Ministry of Education, Science, and Culture, Japan.

References and Notes

(1) Ishida, T.; Tsuboi, H.; Nogami, T.; Yoshikawa, H.; Yasui, M.; Iwasaki, F.; Iwamura, H.; Takeda, N.; Ishikawa, M. *Chem. Lett*. **1994**, 919−922.

(2) (a) Chiarelli, R.; Rassat, A.; Rey, P. *J. Chem. Soc., Chem. Commun*. **1992**, 1081−1082. (b) Chiarelli, R.; Novak, M. A.; Rassat, A.; Tholence, J. L. *Nature* **1993**, *363*, 147−149.

(3) (a) Awaga, K.; Inabe, T.; Nagashima, U.; Maruyama, Y. *J. Chem. Soc., Chem. Commun*. **1989**, 1617−1618; **1990**, 520. (b) Tamura, M.; Nakazawa, Y.; Shiomi, D.; Nozawa, K.; Hosokoshi, Y.; Ishikawa, M.; Takahashi, M.; Kinoshita, M. *Chem. Phys. Lett.* **1991**, *186*, 401−404. (c) Nakazawa, Y.; Tamura, M.; Shirakawa, N.; Shiomi, D.; Takahashi, M.; Kinoshita, M.; Ishikawa, M. *Phys. Rev. B* **1992**, *46*, 8906−8914. (d) Kinoshita, M. *Mol. Cryst. Liq. Cryst*. **1993**, *232*, 1−12.

(4) (a) Mukai, K.; Nedachi, K.; Jamali, J. B.; Achiwa, N. *Chem. Phys. Lett*. **1993**, *214*, 559−562. (b) Mukai, K.; Konishi, K.; Nedachi, K.; Takeda, K. *J. Magn. Magn. Mater*. **1995**, *140*−*144*, 1449−1450. (c) Mukai, K.; Nedachi, K.; Takiguchi, M.; Kobayashi, T.; Amaya, K. *Chem. Phys. Lett*. **1995**, *238*, 61−64. (d) Mukai, K.; Konishi, K.; Nedachi, K.; Takeda, K. *J. Phys. Chem.* **1996**, *100*, 9658−9663.

(5) Togashi, K.; Imachi, R.; Tomioka, K.; Tsuboi, H.; Ishida, T.; Nogami, T.; Takeda, N.; Ishikawa, M. *Bull. Chem. Soc. Jpn.* **1996**, *69*, 2821−2830.

(6) Nogami, T.; Ishida, T.; Yasui, M.; Iwasaki, F.; Takeda, N.; Masayasu, M.; Kawakami, T.; Yamaguchi, K. *Bull. Chem. Soc. Jpn*. **1996**, *69*, 1841−1848.

(7) See, for example, the following. (a) Azuma, N.; Yamauchi, J.; Mukai, K.; Ohya-Nishiguchi, H.; Deguchi, Y. *Bull. Chem. Soc. Jpn*. **1973**, *46*, 2728−2734. (b) Azuma, N. *Bull. Chem. Soc. Jpn*. **1982**, *55*, 1357−1361. (c) Bosch, J.; Molins, E.; Miravitlless, C.; Palacio, F.; Veciana, J. *Mol. Cryst. Liq. Cryst.* **1990**, *187*, 67−74. (d) Dormann, E.; Dyakonow, W.; Gotschy, B.; Lang, A.; Naarmann, H.; Pilawa, B.; Walker, N.; Winter, H. *Synth. Met.* **1993**, *45*−*57*, 3273−3278. (e) Nakamura, T.; Awaga, K.; Inabe, T.; Honda, K.; Matsumoto, M.; Maruyama, Y. *Mol. Cryst. Liq. Cryst*. **1993**, *233*, 105−112. (f) Kremer, R. K.; Kanellakopulos, B.; Bele, P.; Brunner, H.; Neugebauer, F. A. *Chem. Phys. Lett*. **1994**, *230*, 255−259. (g) Mito, M.; Nakano, H.; Kawae, T.; Hitaka, M.; Takagi, S.; Deguchi, H.; Suzuki, K.; Mukai, K.; Takeda, K. *J. Phys. Soc. Jpn*., in press.

(8) (a) Allemand, P.-M.; Srdanov, G.; Wudl, F. *J. Am. Chem. Soc*. **1990**, *112*, 9391−9392. (b) Allemand, P.-M.; Srdanov, G.; Wudl, F. *Synth. Metals* **1991**, *43*, 3245−3248.

(9) Neugebauer, F. A.; Fischer, H.; Krieger, C. *J. Chem. Soc., Perkin Trans. 2*, **1993**, 535−544.

(10) Neugebauer, F. A.; Bernhardt, R. *Chem. Ber*. **1974**, *107*, 529−536.

(11) Bamberger, E.; Padova, R.; Ormerod, E. *Liebigs Ann. Chem*. **1926**, *446*, 260−307. Hubbard, D. M.; Scott, E. W. *J. Am. Chem. Soc*. **1943**, *65*, 2390−2393.

(12) Ashley, J. N.; Davis, B. M.; Nineham, A. W.; Slack, R. *J. Chem. Soc*. **1953**, 3381−3388.

(13) *Enraf-Nonius, CAD-4 Software*, Version 5.1; Enraf Nonius: Delft, The Netherlands, 1992. *Data and LSFM Software*, *1990*; Enraf Nonius: Delft, The Netherlands, 1990.

(14) Burla, M. C.; Camalli, M.; Cascarano, G.; Giacovazzo, C.; Polidori, G.; Viterbo, D. *J. Appl. Crystallogr*. **1989**, *22*, 389−393.

(15) *TEXSAN*−*Texray Structure Analysis Package*, Version 5.0; Molecular Structure Corporation: The Woodlands, TX, 1989.

(16) Atomic coordinates, bond lengths and angles, torsional angles, and thermal parameters have also been deposited at the Cambridge Crystallographic Data Center, England.

(17) Takeda, K.; Wada, M. *J. Phys. Soc. Jpn*. **1981**, *50*, 3603−3611.

(18) Williams, D. E. *J. Am. Chem. Soc*. **1969**, *91*, 1243−1245; *Acta Crystallogr., Sect. B* **1975**, *29*, 96−102.

(19) Azuma, N.; Deguchi, Y.; Marumo, F.; Saito, Y. *Bull. Chem. Soc. Jpn*. **1975**, *48*, 819−824.

(20) Azuma, N.; Deguchi, Y.; Marumo, F.; Saito, Y. *Bull. Chem. Soc. Jpn*. **1975**, *48*, 825−829.

(21) Azuma, N. *Bull. Chem. Soc. Jpn*. **1980**, *53*, 2671−2672.

(22) Azuma, N.; Tsutsui, K.; Miura, Y.; Higuchi, T. *Bull. Chem. Soc. Jpn*. **1981**, *54*, 3274−32 .

(23) Dvorkin, A. A.; Polumbrik, O. M.; Ryabokon, I. G.; Simonov, Yu. A.; Malinovskii, T. I. *Dokl. Akad. Nauk SSSR* **1984**, *277*, 1134−1138.

(24) Bonner, J. C.; Fisher, M. E. *Phys. Rev*. **1964**, *135*, A640−A658.

(25) Steiner, M.; Villain, J.; Windsor, C. G. *Adv. Phys*. **1976**, *25*, 87−209.

(26) Oguchi, T. *Phys Rev*. **1964**, *133*, A1098−A1099.

(27) Lemaire, H.; Rey, P.; Rassat, A.; de Combarieu, A.; Michel, J.-C. *Mol. Phys*. **1968**, *14*, 201−208.

(28) Chouteau, G.; Veyret-Jeandey, C. *J. Phys. (Orsay, Fr.)* **1981**, *42*, 1441−1444.

(29) Kobayashi, T.; Takiguchi, M.; Amaya, K.; Sugimoto, H.; Kajiwara, A.; Harada, A.; Kamachi, M. *J. Phys. Soc. Jpn.***1993**, *62*, 3239−3243.

(30) Togashi, K.; Imachi, R.; Tomioka, K.; Tsuboi, H.; Ishida, T.; Nogami, T.; Takeda, N.; Ishikawa, M. *Bull. Chem. Soc. Jpn*. **1996**, *69*, 2821−2830.

(31) Yamauchi, J.; Adachi, K.; Deguchi, Y. *J. Phys. Soc. Jpn*. **1973**, *35*, 443−447.

(32) Takeda, K.; Yoshino, Y.; Matsumoto, K.; Haseda, T. *J. Phys. Soc. Jpn*. **1980**, *49*, 162−169.

(33) Bonner, J. C.; Blote, H. W. J.; Bray, J. W.; Jacobs, I. S. *J. Appl. Phys*. **1979**, *50*, 1810−1812.

(34) Azuma, N. *Bull. Chem. Soc. Jpn*. **1982**, *55*, 1357−1361.

(35) Nakamura, T.; Awaga, K.; Inabe, T.; Honda, K.; Matsumoto, M.; Maruyama, Y. *Mol. Cryst. Liq. Cryst*. **1993**, *233*, 105−112.

(36) Mukai, K.; Kawasaki, S.; Jamali, J. B.; Achiwa, N. *Chem. Phys. Lett*. **1995**, *241*, 618−622.

(37) Mukai, K.; Wada, N.; Jamali, J. B.; Achiwa, N.; Narumi, Y.; Kindo, K.; Koboyashi, T.; Amaya, K. *Chem. Phys. Lett*. **1996**, *257*, 538−544.